Poincaré maps of Duffing-type oscillators and their reduction to circle maps: II. Methods and numerical results

1998 J. Phys. A: Math. Gen. 31 3903

(http://iopscience.iop.org/0305-4470/31/16/017)

J. Phys. A: Math. Gen. **31** (1998) 3903–3927. Printed in the UK PII: S0305-4470(98)87398-8

Poincaré maps of Duffing-type oscillators and their reduction to circle maps: II. Methods and numerical results

K Schmidt† and G Eilenberger‡

† EDS Electronic Data Systems Fertigungsindustrie (Deutschland) GmbH, Eisenstraße 58, D-65424 Rüsselsheim, Germany

‡ Institut für Festkörperforschung, Forschungszentrum Jülich, D-52425 Jülich, Germany

Received 8 September 1997

Abstract. Bifurcation diagrams and plots of Lyapunov exponents in the r–Ω plane for Duffing-type oscillators

$$\ddot{x} + 2r\dot{x} + x^q = f(x, \Omega t)$$

exhibit a regular pattern of repeating self-similar 'tongues' with complex internal structure. We demonstrate here how this behaviour is easily understood qualitatively and quantitatively from a Poincaré map of the system in action-angle variables in the limit of large driving force or, equivalently, small driving frequency. This map approaches the *one-dimensional* form

$$\varphi_{n+1} = \alpha + \beta\cos\varphi_n$$

as derived in paper I.

This second paper describes our approach to calculating the various constants and functions introduced in paper I. It gives numerical applications of the theory and tests its range of validity by comparison with results from the numerical integration of Duffing-type equations. Finally we show how to extend the range in the parameter space where the map is applicable.

1. Introduction

The Duffing oscillator

$$\ddot{X} + 2R\dot{X} + X^3 + X = F\cos w\tau \tag{1}$$

is known to show many nonlinear phenomena like multiple resonances, bifurcations and chaos. A numerically calculated diagram of bifurcation lines in parameter space (figure 1) shows a regular pattern of similar stripes each of which consists of 'tongues' which denote bifurcation cascades leading to chaotic time evolution.

The dynamics of the system always combines motion following the driving force and oscillations with an internal frequency. Each stripe is characterized by a fixed number n of internal oscillations during one period of the driving force (figure 3). For large n the tongues become increasingly similar to each other and approach an asymptotic generic pattern which we expect to become particularly amenable to analysis and at which our investigation is primarily aimed.

As in paper I† [1]‡ we therefore investigate the case of large driving amplitudes F. In this case, because of the potential's stiffening nonlinearity, the internal oscillations become

† References to formulae of paper I will be denoted by (I, ...).

‡ In (I, 5.27) the second line should read: $= \varphi_a + e^{-rT}(1 + 1/2e^{-rT}i_n)C_1\cos(\varphi_n + \psi_1) + e^{-2rT}[C_2\cos(2\varphi_n + \psi_2) + C_3]$.

0305-4470/98/163903+25$19.50

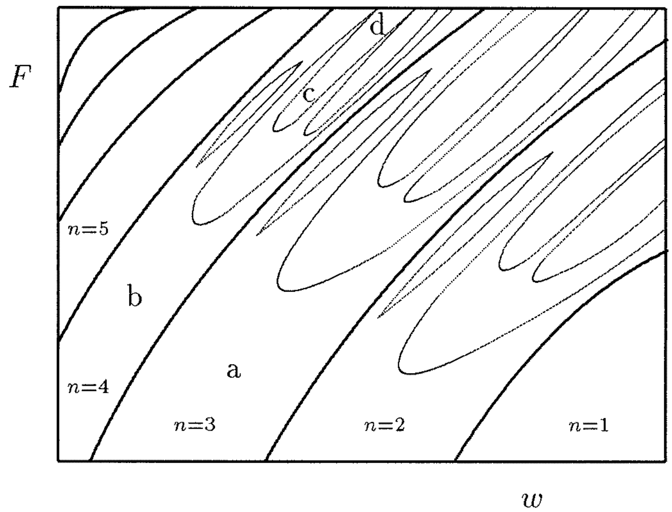

Figure 1. Schematic phase diagram of Duffing's equation. Heavy curves separate stripes of resonance order n, light curves denote bifurcation cascades. A path through the diagram along increasing driving force amplitude F crosses several bifurcation lines and eventually leads into chaotic regions. The letters a to d refer to figure 3.

faster and faster compared to the frequency of the driving force.

For analytic purposes, however, it is more convenient to rescale according to

$$a = F^{1/3} \qquad x = \frac{X}{a} \qquad t = a\tau \qquad \Omega = \frac{w}{a} \qquad r = \frac{R}{a} \tag{2}$$

to obtain

$$\ddot{x} + 2r\dot{x} + x^3 + \frac{1}{a^2}x = \sin \Omega t. \tag{3}$$

This means that now the amplitude and internal frequency remain of order 1, whereas the driving frequency becomes smaller as F in equation (1) increases. It is important that the scaling (2) leaves the ratio $R/w = r/\Omega = c$ unchanged. This ratio c constitutes, besides Ω, the second independent parameter. The linear term in equation (3) becomes irrelevant in the limit of large a; we therefore considered only Duffing-'type' models without a linear term in the restoring force.

Equation (3) can be viewed as a special case of the general class of oscillators

$$\ddot{x} + 2r\dot{x} + V'(x, \Omega t) = 0 \tag{4}$$

where the total potential $V(x, t)$ has only one minimum in x and is periodic in t. In paper I we have shown how our analytic theory can be applied to this class. We concentrate here on typical particular cases of the form

$$\ddot{x} + 2r\dot{x} + x^q = x^l \sin^p \Omega t \tag{5}$$

with positive real exponents (p, q, l) as in paper I. To obtain an intuitive picture one may consider the case of odd $q > 1$, $l = 0$, $p = 1$.

Forced Duffing-type oscillators are systems, which allow a simple physical interpretation of their equation of motion and at the same time they exhibit a wealth of complex phenomena characteristic for nonlinear science. There are currently several active lines of study into different aspects of these systems.

There is the frictionless Duffing oscillator; in a sense a minimalistic yet realistic Hamiltonian model system in which to study the effects of tori breaking and KAM theory [2]. For our considerations friction, however small, must not vanish; we do not contribute to a better understanding of Hamiltonian systems here.

For dissipative Duffing systems the next dichotomy is between double- (or multiple-) well oscillators and single-well oscillators. In the former, the cause for bifurcations and chaos in case of not too large driving forces is more obvious, but these phenomena seem nevertheless more involved and quantitatively more difficult to understand [3] than in the latter case, which we treat exclusively. Among the former, the extensive work of Gilmore and McCallum [4] contains some connection with ours in that they derive one- and two-dimensional return maps including maps of the circle. The physical mechanism underlying these maps does not seem to be related to ours, however.

The driving force can be considered deterministic or noisy. In the latter case the topic becomes a subject of statistical physics [5]. We consider deterministic periodic driving only in the limit of large amplitudes (or, equivalently, small frequencies). However, several of the methods developed here are expected to be applicable to other types of driving forces, quasiperiodic ones for instance, which have been subject to several studies [6]. We have briefly dwelt on this question in (I, section 6).

Finally, being interested in *large* forcing amplitudes, our investigation is complementary in parameter space to investigations where different methods like pertubation theory, averaging methods or Fourier series, to name just a few, are effective [7].

We have not touched upon the question of controlling [8] or coupling [9] Duffing oscillators, also active topics of research. We believe, however, that our intuitive picture induced by the oscillator's Poincaré map may also open new roads of research into these topics.

We found almost no investigation in the literature with aims, methods or results related to ours. Only the work by Stefanescu [10], available as an unpublished report, derives some of our results (though by different methods) with the aim of understanding the self-similarity and generic internal bifurcation structure in the parameter plane at large amplitudes. Stefanescu arrives at the same one-dimensional map of the circle for this limiting case, without giving explicit analytical formulae for the coefficients.

There is a great wealth of numerical work on this bifurcation structure, the most comprehensive being Ueda's [11]. Furthermore, there are numerical studies concerning particular questions on Duffing-type systems, for instance [12]. In our opinion, a majority of these results could be classified systematically and understood qualitatively and semiquantitatively (even in an intermediate amplitude regime) by relating them to our map.

The map in which the term linear in φ_n is absent is very different in effect to the usually so-called 'circle map', for which a vast literature exists; our map falls instead into the Feigenbaum class of maps [13]. An important aspect of our particular specimen from this class is the periodicity of the cosine and hence multiplicity of attractors for larger values of β. This aspect of the cosine map has not been closely investigated to our knowledge, nor has the multiplicity of attractors in the far chaotic regime of Duffing-type systems, which is explained by the former.

In the following we shall summarize the main ideas and results of paper I. The main body of the present paper contains the numerical and technical methods used to apply our theory and numerical checks of its accuracy and limits. The corresponding programs are documented in [14] and are available on ftp://ftp.fz-juelich.de.

We shall construct a Poincaré map of the system by transforming the Duffing oscillator into a system with a time-dependent potential, the nonlinear parts of which decay during each half-period $\pi/\Omega = T$ due to friction. We succeed in describing the cumulative effect on the Poincaré map of the nonlinearity by a set of 'universal' constants which for large values of n are independent of the system parameters (r, Ω) (but do depend on the general shape of the potential V in (4)).

As a first step towards the construction of the Poincaré map we define special 'reference solutions' $x_0(t)$ for equation (5) with the property of varying only on the same time scale as the driving force but not oscillating in the potential well. We show numerically that such solutions do exist during each half-period T between two zeros of the driving force, but that they start oscillating if continued beyond one half-period. The reason for the latter is that these solutions follow essentially the motion of the minimum $x_m(t)$ of the total potential $V(x,t)$. This minimum is flat when $\sin\Omega t$ vanishes; at this instance the minimum moves with momentarily infinite speed and the connection between $x_0(t)$ and $x_m(t)$ is broken.

Arbitrary solutions $x(t)$ are attracted by $x_0(t)$ during the corresponding half-period, i.e. $y = x - x_0$ decays as a consequence of friction (figure 2). The important feature of x_0—not to oscillate—leads to an equation of motion for y with slowly varying coefficients in its potential $W(y, x_0(t))$, the minimum of which is now stationary at $y = 0$ by construction. This allows application of the adiabatic theorem in a next step. If x_0 were extended beyond one half-period, we would lose this essential advantage. Therefore we define one function x_0 for the even, another one for the odd half-periods, these solutions belonging to *different*

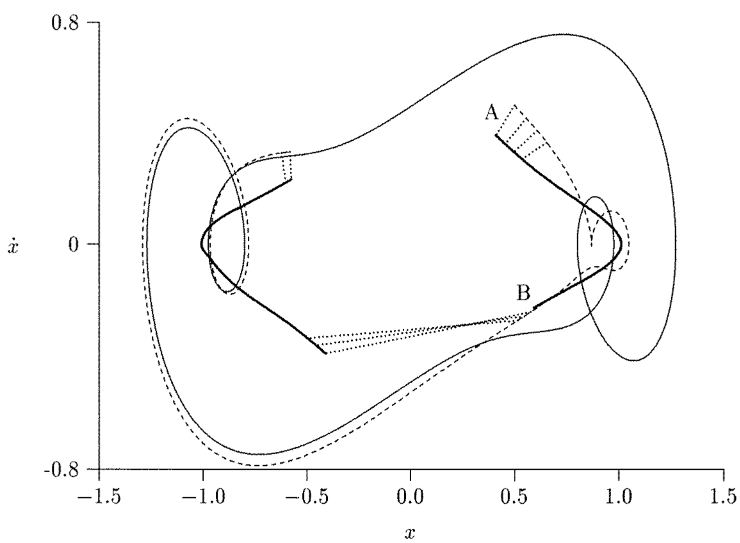

Figure 2. Three solutions of Duffing's equation. Transient solution $x(t)$ (- - - -) leading to the limit cycle (——). Reference solution $x_0(t)$ (heavy curve). Some points belonging to the same time instant are connected $(\cdots\cdots)$. Point A ($t = 0$): the right branch of x_0 starts. The solution $x(t)$ is attracted by $x_0(t)$, *not* by the limit cycle. At B ($t = T$) the right branch of x_0 ends and $x(t)$ has closely approached $x_0(t)$. The next reference point now belongs on the left branch, this constitutes the kick which restarts decaying oscillations about the new reference solution. The net result of these repeating kicks and decays is—in this particular case—the limit cycle. Parameters: $r = 0.275$; $\Omega = 0.35$; $q = 3$.

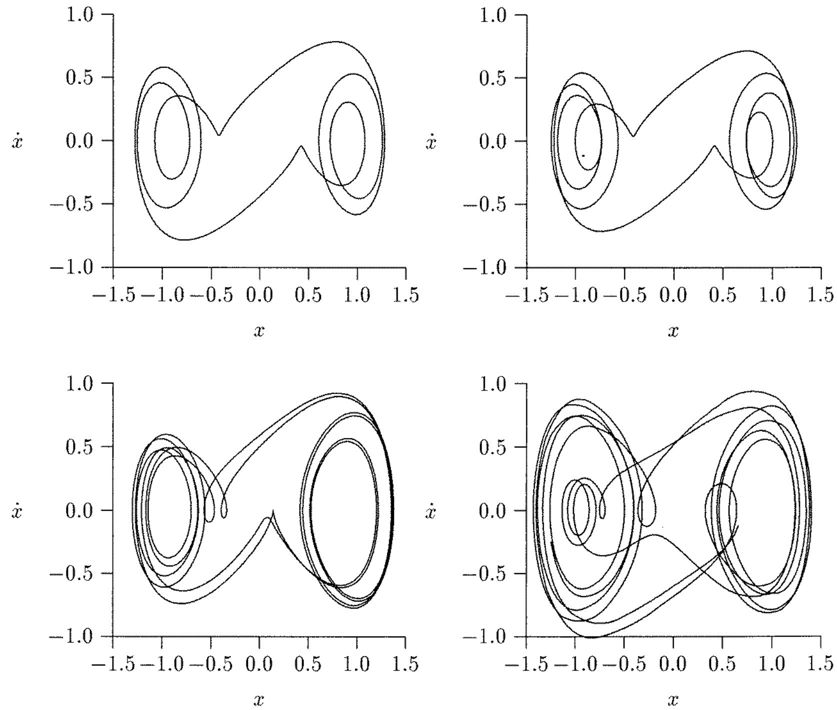

Figure 3. Phase portraits for four parameter sets denoted by 'a' to 'd' in figure 1. Top left: $n = 3$, simple periodic orbit, 'a'. Top right: same state as top left, but next resonance, $n = 4$, 'b'. Bottom left: same resonance as top left, but after the first (left–right symmetry breaking) bifurcation, $n = 3$, 'c'. Bottom right: chaotic orbit, $n = 3$, 'd'.

initial conditions for the equation (5)†. This leads to discontinuities in the coefficients of the differential equation for y at times $t_m = mT$. The discontinuities constitute a 'kick' which injects potential energy into the y-system at times mT and periodically restarts internal oscillations (figure 3). This is the mechanism which produces the nonlinear effects; it is missing in the corresponding driven *harmonic* oscillator.

The technical possibility to analytically and explicitly construct a Poincaré map rests on two features of the problem as discussed in paper I. First, the transformation $z = \mathrm{e}^{-rt} y$ of the difference coordinate y eliminates the friction in its equation of motion: the system becomes Hamiltonian. Introducing action-angle variables (I, φ), the action I is then constant due to the adiabatic theorem provided r is small, $x_0(t)$ is slowly varying and the minimum of $W(y, x_0(t))$ is stationary at $y = 0$. Equally well though, one may keep the dissipative y-system and translate the invariability of the Hamiltonian action I into the relation $I(t_1) = \mathrm{e}^{-2r(t_2-t_1)} I(t_2)$ for the dissipative system.

The second feature is the homogeneity of order $q + 1$ of the potential $W(y, x_0(t))$ as a function of y and x_0 for most of each half-period T. As shown in paper I, this allows an explicit expansion of the frequency $\omega(I(t), x_0(t))$ into powers of $I(t)$

$$\omega(I, x_0) = c_1 x_0^{\frac{q-1}{2}} + 2c_2 x_0^{-2} I + 3c_3 x_0^{-\frac{q+7}{2}} I^2 + \cdots \tag{6}$$

with known factors c_ν. This permits the explicit solution for $\varphi(t)$.

† We keep and use the symmetry $(x, \dot{x}, t) \to (-x, -\dot{x}, t + T)$ throughout this paper.

Thus an explicit construction of the Poincaré map as a series in powers of e^{-rT} is achieved, which to *first* order has the simple form

$$\varphi_{n+1} = \alpha + \beta \cos \varphi_n. \tag{7}$$

This map determines qualitatively and nearly quantitatively all the nonlinear effects one might obtain in the large forcing limit from the Duffing-type equations considered. The quantity α which roughly increases like T causes the repeating pattern in the bifurcation diagram and defines the 'resonance order' n discussed earlier. The 'nonlinear strength' $\beta \sim C(r, T)e^{-rT}$ measures the coordinate in parameter space along the tongues with their bifurcation cascades, regions of chaotic motion and multiple attractors.

The parameters α and β in equation (7) constitute coordinates in parameter space, which most clearly exhibit the near periodicity of the bifurcation diagram and the adiabatic structure of the tongues. Translating back into the original parameters F and $c = R/w$ of the generalized Duffing's equation (5), we obtain in the large c limit

$$\alpha \sim F^{\delta} \qquad \beta \sim F^{\sigma} c^{\zeta} e^{-\pi c} \tag{8}$$

where δ, σ and ζ depend on the exponents (p, q, l). For the original Duffing case $(p, q, l) = (1, 3, 0)$ we have $\delta = \frac{1}{3}$, $\sigma = \frac{1}{12}$, $\zeta = -\frac{1}{3}$.

To *second* order we obtained a two-dimensional I–φ map of the type

$$\begin{aligned} \varphi_{n+1} &= \Phi_0 + e^{-rT}\Phi_1 + e^{-2rT}\Phi_2 \\ i_{n+1} &= W_1 + e^{-rT} W_2 \end{aligned} \tag{9}$$

where

$$\begin{aligned}
\Phi_0 &= \varphi_a + A_1 T + \sum_{\nu=2}^{N} A_\nu F_\nu(r, \Omega) \\
\Phi_1 &= B_1 \sum_{\nu=2}^{N} (\nu - 1) A_\nu F_\nu(r, \Omega) \cos(\varphi_n + \chi_1) + C_1 \cos(\varphi_n + \psi_1) \\
\Phi_2 &= \sum_{\nu=2}^{N} (\nu - 1) A_\nu F_\nu(r, \Omega)[B_2 \cos(2\varphi_n + \chi_2) + B_3 + \tfrac{1}{2}(\nu - 2) B_1^2 \cos^2(\varphi_n + \chi_1) \\
&\qquad + \tfrac{1}{2} B_1 i_n \cos(\varphi_n + \chi_1)] + \tfrac{1}{2} C_1 i_n \cos(\varphi_n + \psi_1) + C_2 \cos(2\varphi_n + \psi_2) + C_3 \\
W_1 &= B_1 \cos(\varphi_n + \chi_1) \\
W_2 &= \tfrac{1}{2} B_1 i_n \cos(\varphi_1 + \chi_1) + B_2 \cos(2\varphi_n + \chi_2) + B_3.
\end{aligned} \tag{10}$$

The upper summation index N is defined in paper I. In all cases considered here we have $N = 2$, the sums consisting of one term only. The quantities α and β introduced in equation (7) are rigorously defined through Φ_0 and Φ_1. In these expressions the dependence of the map on the dynamic variables *and* on the parameters (r, Ω) is given explicitly. In the following we shall describe our strategy to determine the universal (i.e. parameter independent) constants φ_a, I_a, A_ν, B_ν, C_ν, ψ_ν and χ_ν and demonstrate the accuracy and range of validity of this map. The F_ν are known functions derived in paper I. In the limit $c = r/\Omega \gg 1$ these functions depend on the parameters as $F_\nu \sim \Omega^{-\kappa_\nu(1-\eta)} c^{-\kappa_\nu}$ with exponents κ_ν as given in paper I.

The important feature of this map is its near one dimensionality given in equation (7). The action variable varies only slightly under the map, being described by

$$I_n = \Omega^{2\gamma+\eta} I_a (1 + e^{-rT} i_n) \tag{11}$$

at the beginning of each half-cycle in the (x, t) scale (in the (ξ, τ) scale the factor $\Omega^{2\gamma+\eta}$ is absent—see the footnote in section 3. Equations (10) contain the information needed for the conversion $(\alpha, \beta) \leftrightarrow (r, T)$ which links the parameters used later for the map to those of the differential equation and thus explicitly gives the quantitative correspondence between the two.

2. The reference solution

We are looking for a solution $x_0(t)$ of equation (5) which oscillates as little as possible in the 'cup' of the total potential

$$V(x,t) = \frac{1}{q+1}x^{q+1} - \frac{1}{l+1}x^{l+1}\sin^p \Omega t \tag{12}$$

during one half-period of the driving force.

We expect that the minimum of the potential

$$x_m = \sin^\delta \Omega t \qquad \delta = \frac{p}{q-l} < \frac{1}{2} \tag{13}$$

is very close to the function x_0 for most of the half-cycle, but x_m cannot be a good approximation for x_0 near $t = mT$, because its time derivatives are divergent at this instant.

The inequality $\delta < \frac{1}{2}$, which was assumed in paper I, is required to obtain at least one relevant term, i.e. $N \geqslant 2$, in the sums of equation (10). For $\delta > 1$ one would obtain quite a different behaviour of the system in its parameter space: the order n would increase with *decreasing* amplitude F. Not unexpectedly, the harmonic oscillator is among the borderline cases $\delta = 1$. We do not know how systems with an intermediate exponent $\frac{1}{2} < \delta < 1$ behave.

In paper I, we considered the reference solution x_0 in the limit $\Omega \to 0$ when the driving force $\sin \Omega t$ may be linearized. This allows us to eliminate Ω by rescaling which leads to the differential equation (I, 4.18)

$$\ddot{\xi} + 2\rho\dot{\xi} + \xi^q = \xi^l \tau^p \tag{14}$$

with the scaling

$$x(t) = \Omega^\gamma \xi(t) \qquad \dot{x}(t) = \Omega^{\gamma+\eta}\xi(t) \qquad t = \Omega^{-\eta}\tau \qquad \rho = r\Omega^{-\eta} \tag{15}$$

where the exponents are given by

$$\eta = \frac{(q-1)\delta}{2+(q-1)\delta} \qquad \lambda = 2 + (q-1)\delta \qquad \gamma = \frac{2\delta}{2+(q-1)\delta}. \tag{16}$$

We approximated the solution by the asymptotic series

$$\xi_0(\tau) = \tau^\delta \left(1 + \sum_{n=1}^{\infty} P_n \tau^{-n\lambda}\right) \tag{17}$$

with polynomials P_n of maximal order n in the variable $\rho\tau$, to be determined order by order from equation (14). It is sufficient to use the first order (which does not contain the friction ρ):

$$\xi_0(\tau) \approx \tau^\delta \left(1 - \frac{\delta(\delta-1)}{q-l}\tau^{-\lambda}\right) \qquad \dot{\xi}_0(\tau) \approx \delta\tau^{\delta-1}\left(1 - \frac{(\lambda-\delta)(1-\delta)}{q-l}\tau^{-\lambda}\right) \tag{18}$$

at an initial time $\tau = 1000$ to obtain an accuracy of 8 digits for $\xi_1 := \xi_0(0)$, $\xi_2 := \dot{\xi}_0(0)$. The numerical integration back to $\tau = 0$ was done with a relative tolerance of 10^{-12}. In appendix A the values of ξ_1 and ξ_2 are listed for various sets of the exponents (p, q, l).

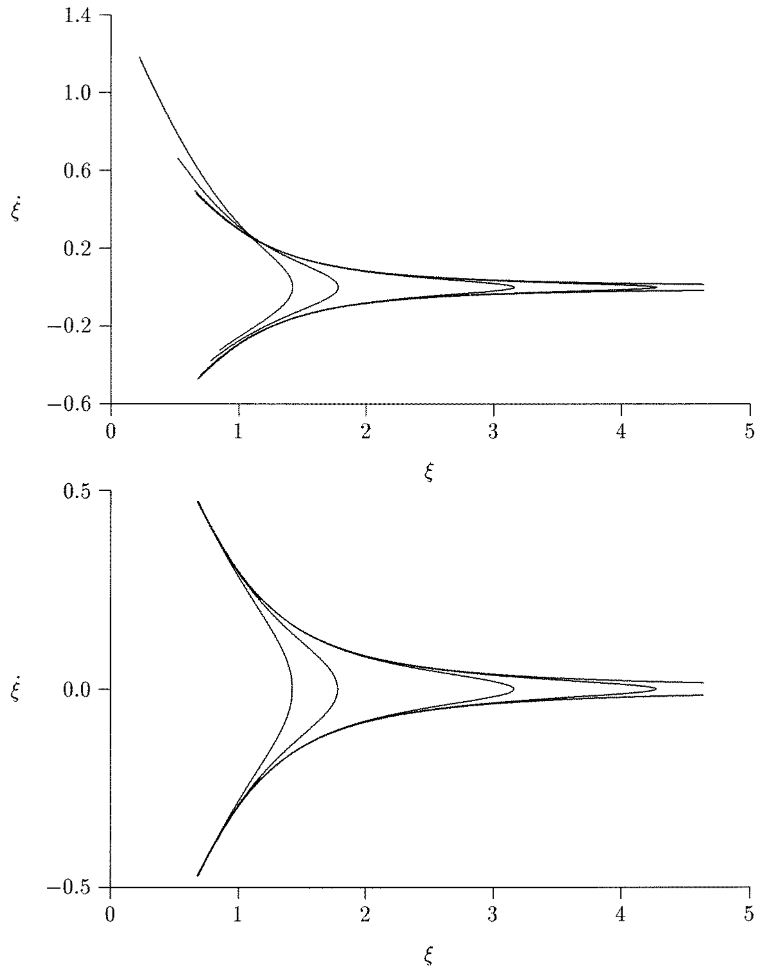

Figure 4. Reference solutions x_0 for $q = 3$, $p = 1$, $l = 0$. Top, from left: $r = 1, 0.4, 0.04, 0.012$; $\Omega = 0.25, 0.1, 0.01, 0.003$. These values correspond to $\rho = 2$. Bottom: Same Ω values and $r = 0$. The trajectories are in ξ scaling. The curve open at the right depicts $\xi_0(\tau)$ for $\rho = 0$.

The reference solution so obtained is the asymptotic limit for $\Omega \to 0$ of the reference solutions for finite (r, Ω) and is smoothly approached by the latter (figure 4), if these are appropriately scaled by powers of Ω. In the case of finite (r, Ω) one cannot eliminate Ω by rescaling and has to consider the full equation (5). Similarly to the limiting case $\Omega \to 0$, we approximate the solution by a series

$$x_0(t) = s^\delta \left(1 + \sum_{n=1}^{N} a_n \Omega^{2n} s^{-n\lambda} \right) \tag{19}$$

with polynomials $a_n(c, sr/\Omega)$ of the variables $s = \sin \Omega t$, $c = \cos \Omega t$. The a_n can be determined from equation (5). The initial conditions for the numerical integration are most conveniently chosen at the instant $t = T/2$ where the deviation of x_0 from s^δ is expected to be smallest. For this use of the series (19), which most likely is an asymptotic series, the question arises how many terms N one needs to sum in order to obtain a desired numerical

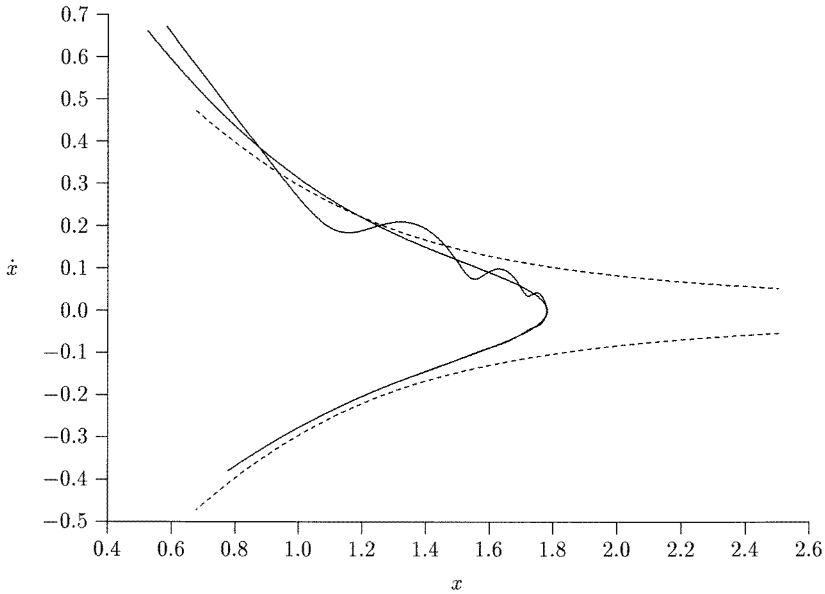

Figure 5. Approximations to x_0 for parameters $(p, q, l) = (1, 3, 0)$, $\Omega = 0.1$, $r = 0.2$ calculated with three methods: Universal solution ξ_0 (- - - -); initial conditions calculated with the procedure described in the text (——); initial conditions $x(T/2) = 1$, $\dot{x}(T/2) = 0$ lead to an oscillating curve (——). For $\Omega \to 0$, $r \approx \Omega$ all three trajectories will converge.

accuracy. Summing up to the term of index $N = N_0$ which is the smallest for a given value Ω might be impractical for small values Ω and would create the problem that N_0 changes as Ω varies; this would cause $x_0(t)$ to vary discontinuously with Ω. Instead we used the Levin transformation T_n [15] to order 10 to obtain reliable values. It is an amazing numerical fact that this increases the accuracy vastly and gives a smooth dependence of x_0 on the parameters (r, Ω).

The requirement that x_0 must not oscillate leaves a small but finite uncertainty in the selection of initial conditions as long as Ω is finite. Numerically, the freedom of choice is *very* small indeed as demonstrated in figure 5. Nevertheless we found no stringent *mathematical definition* for the construction of x_0. Our procedure *constructively* defines x_0 by using the Levin transformation to obtain initial conditions at $T/2$ for numerical integration. This is consistent with the asymptotic series (17) to which $x_0(t, \Omega)$ converges in the limit $\Omega \to 0$ if scaled as in equations (15). A selection of reference solutions for different sets (p, q, l) is shown in figure 6.

We used automated formula manipulation techniques to obtain to order 10 the polynomials P_n and a_n for the series (17) and (19) resp. [14].

3. Determination of map coefficients

The formulae for the Poincaré map are derived under the assumption that Ω can be considered arbitrarily small when necessary and that r scales as Ω with $c = r/\Omega > 1$ held fixed.

In this asymptotic regime the reference solution and the difference system y have the following relevant properties: near the 'ends' of each half-cycle (corresponding to the

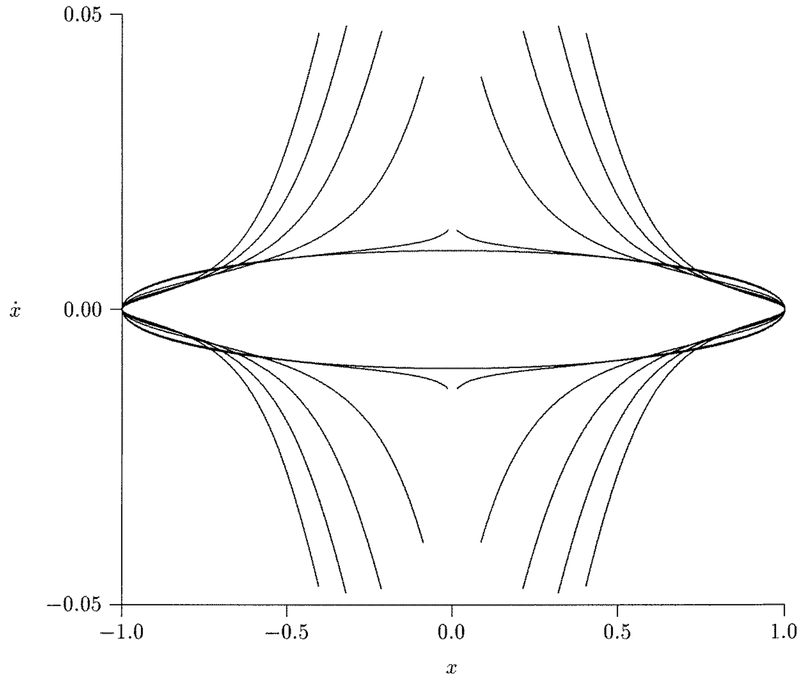

Figure 6. Reference solutions $x_0(t)$ for different exponents q, $p = 1$, $l = 0$, at parameter values $r = 0$, $\Omega = 0.01$ in x, t scaling. From the outside: $q = 5, 4, 3, 2, 1.1, 1$. At $q = 1.1$, which is near the harmonic value $q = 1$ the deviation from the harmonic cycle is very small but visible. The opening between the two branches for $q = 1.1$ is exaggerated here for visibility; actually it is minute but not vanishing. Increasing values of q lead to larger openings between the two branches of x_0, the effects of the kick increases correspondingly.

regions I and V of figure 7) the reference solution has approached the limiting reference solution† ξ_0, of equation (14) as demonstrated in figure 4. For time intervals $\Delta t = \Omega^{-\varepsilon}$ (with any $\varepsilon < 1$) friction can be neglected entirely because $r\Delta t$ becomes arbitrarily small with Ω. Thus numerical solutions for the difference system y in this time regime are *universally* valid for all values of r and Ω if only scaled appropriately by powers of Ω.

In the ‘middle’ of each cycle, on the other hand, the reference solution is so close to $x_m(t)$, the minimum position, that x_0 can be replaced by x_m which then leads to a total potential $W(y, x_m)$ homogeneous of order $q + 1$ in the variables y and x_m as mentioned earlier. At the same time $x_0(t)$ varies so slowly that the adiabatic theorem applies. Finally, well into each half-cycle, the action I as expansion parameter has decayed by a factor of about e^{-rT} which was assumed to be small. This fact conspires, together with the smallness of x_m at the *beginning* of each half-cycle (where I is *not* small in general), to yield fast convergence of the series of integrals for $\varphi(t) = \int \omega(I(t), x_0(t))\, dt$ which is generated by the expansion (6) of ω into powers of I.

In overlapping regions between the middle and the ends we can patch together the universal numerical solutions from the ends (which yield the parameter free numerical constants) with the explicitly available analytic solution for the middle region and so obtain the complete evolution for one half-cycle in the form of a Poincaré map.

† In the following we often switch without explicit mention between the (x, t) and (ξ, τ) scales, which are connected via (15).

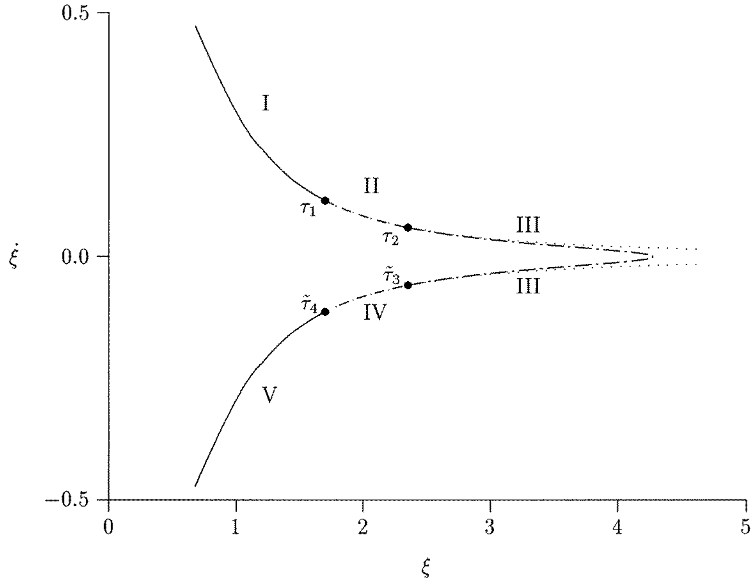

Figure 7. Different regions in the reference solution of Duffing's equation in (ξ, τ) scaling as described in the text.

Table 1. Properties of the reference solution during different time intervals stated in the text.

Region	$\xi \to$	Adiabatic	Homogeneous
I	ξ_0		
II	$\xi_0 \to \tau^\delta \leftarrow s^\delta$	×	×
III	s^δ	×	×
IV	$\xi_0 \to \tau^\delta \leftarrow s^\delta$	×	×
V	ξ_0		

The division of the half-cycle T into these different intervals is defined by time instants

$$\tau_1 = \Omega^{-\epsilon} \qquad \tau_2 = \Omega^{-2\epsilon} \qquad \tau_3 = T - \tau_2 \qquad \tau_4 = T - \tau_1 \tag{20}$$

which are somewhat arbitrarily choosen with $\epsilon = (1 - \eta)/3$, such that $\mathrm{e}^{-\rho\tau_2} \to 1$ and such that corresponding values of the variable ξ behave as

$$\xi(\tau_1) \to \infty \qquad \xi(\tau_2) \to \infty \qquad \frac{\xi(\tau_2)}{\xi(\tau_1)} \to \infty \tag{21}$$

in the limit $\Omega \to 0$. This divides T into five intervals consecutively numbered I to V. The system's behaviour in these intervals is listed in table 1. In the overlapping regions II and IV *all* conditions necessary to patch the numerical and analytical solutions together are fulfilled (see figure 7).

The constants are determined in two steps, which relates to the fact that, at the *beginning* of each half-cycle, the coordinates $(x, \dot{x})$ will be very close to the endpoint of the *last* reference cycle $(x_0(T), \dot{x}_0(T))$ which had attracted the trajectory under consideration. It is actually this *difference* which is the object of the Poincaré map.

In a first step, we start a particular trajectory at $\tau = 0$ *precisely* with the initial conditions $(\xi, \dot{\xi}) = (-\xi_1, \xi_2)$ from the endpoint of the *previous* branch of ξ_0. We integrate it numerically to some time $\tau = \tau_+$ inside region II, where we transform the variables $(\xi, \dot{\xi})$ into action-angle variables (I, φ) as described in paper I. From here on, into region IV, the time evolution of (I, φ) is given analytically by

$$I(t) = \mathrm{e}^{-2rt}\Omega^{2\gamma+\eta} I_a \qquad \varphi(t) = \varphi_a + \int_0^t \omega(I(t), x_m(t))\,\mathrm{d}t \tag{22}$$

(note the index m in the argument of ω). The initial conditions (I_a, φ_a) of this particular trajectory are determined through insertion into (22) of the numerically determined values at some instant τ_+ inside region II. Obviously, the precise value of τ_+ inside region II must be irrelevant, if the patching procedure is to make sense. This provides a numerical test of the validity of our arguments. The values (I_a, φ_a) are 'fictitious' initial conditions at $t = 0$, in the sense that they would generate an identical trajectory in the middle region if the system were evolving according to (22) everywhere.

As any solution in action angle variables of the y-system is given by (22) inside regions II through IV (with some values replacing the particular I_a, φ_a) we can assign fictitious action-angle variables to any given solution in the intervals I and V by extrapolation of (22) along the trajectory. *The variables of our Poincaré map are the values of these fictitious variables at the end of each half-cycle*. In region IV near $t = T$, the action I of any trajectory which started near (fictitious) (I_a, φ_a) at $t = 0$ (i.e. *near* the endpoint of the previous reference solution) has decayed to $I(t) \approx I_a \mathrm{e}^{-2rT}$. Consequently the system has become nearly harmonic, which means that the (true) difference cordinates are determined through the (ficticious) action-angle variables approximately by

$$y(T) \sim u_1 + u_2 \qquad \dot{y}(T) \sim \frac{u_1 - u_2}{\mathrm{i}} \qquad u_{1/2} = \mathrm{e}^{-rT}\sqrt{I_a}\,\mathrm{e}^{\pm \mathrm{i}\varphi(T)}. \tag{23}$$

As this trajectory continues through the next cycle, the difference coordinates (23) will determine the deviation from I_a, φ_a of the new initial values $I(0)$ and $\varphi(0)$ (with the clock set back to 0†). Since this deviation is small of order e^{-rT}, we may expand to second order (using summation convention):

$$\begin{aligned} I(0) &= I_a + K_\nu u_\nu + \tfrac{1}{2} K_{\nu\mu} u_\nu u_\mu \\ \varphi(0) &= \varphi_a + P_\nu u_\nu + \tfrac{1}{2} P_{\nu\mu} u_\nu u_\mu. \end{aligned} \tag{24}$$

The constants K, P in equation (24) contain all information on the desired Poincaré map. These constants are now determined in a second step.

For 24 conveniently spaced pairs of fictitious 'final' coordinates (I_k, φ_k) at time T we determined the coordinates $(y_k, \dot{y}_k)$ at some time $T - \tau_+$ in region IV and used these as initial conditions to integrate numerically trajectories from $-\tau_+$ to τ_+ to obtain the corresponding (fictitious) initial conditions $(I_k(0), \varphi_k(0))$ for the next cycle. From these, the 10 constants in equation (24) have been obtained by a least squares fit.

The method described encounters the technical problem that the usual canonical transformation $(I, \varphi) \leftrightarrow (\xi, \dot{\xi})$ as described in paper I is of sufficient accuracy only for a system which is *very* nearly adiabatic in regions II–IV. This would require very large values τ_+ (corresponding to very small values Ω) and thus very large intervals $[-\tau_+, \tau_+]$ for the numerical integration (an interval $[-10^7, 10^7]$ would lead to only three digit accuracy in the map coefficients). Instead we used an action-angle transformation (described in appendix B) which takes into account the explicit time dependence of the potential $W(y, x_0)$.

The map coefficients are then obtained to six digits accuracy by integrating trajectories along the interval $\tau = [-200, 200]$. The integrations were done with a tolerance of 10^{-18}.

† We make use of the earlier mentioned inversion symmetry of our system.

We have thereby determined coefficients for a wide range of model exponents (p, q, l). In appendix A a table for a few characteristic cases is given.

4. The Poincaré map with finite r and Ω

So far, we have not discussed what an 'asymptotic regime' means in actual numbers. We shall now explore the reliability and limits in parameter space of our theory numerically and test possible extensions.

To this end, we calculated and compared diagrams in parameter space of the Lyapunov exponents by alternatively integrating the differential equation itself and iterating the Poincaré map in its one- and two-dimensional form on a mesh of parameter values. We consider the quantities α and β as derived from the expressions Φ_0 and Φ_1 in equations (10) as particularly suitable coordinates in parameter space; in these coordinates the near identity of the periodically repeated tongues in the 'Lyapunov diagrams' is most clearly seen. The deviation from full periodicity is supposedly caused by the second (and possibly higher) order terms of the map.

Figure 8 graphically demonstrates the relation between the coordinates (α, β) and (r, T) in parameter space for the case $(p, q, l) = (1, 3, 0)$. For other exponents, it looks qualitatively the same.

Figures 9 and 10 compare Lyapunov diagrams for Duffing's equation ($(p, q, l) = (1, 3, 0)$) with the diagrams for the corresponding one- and two-dimensional maps. The area in parameter space covered by this diagram obviously belongs to the asymptotic regime

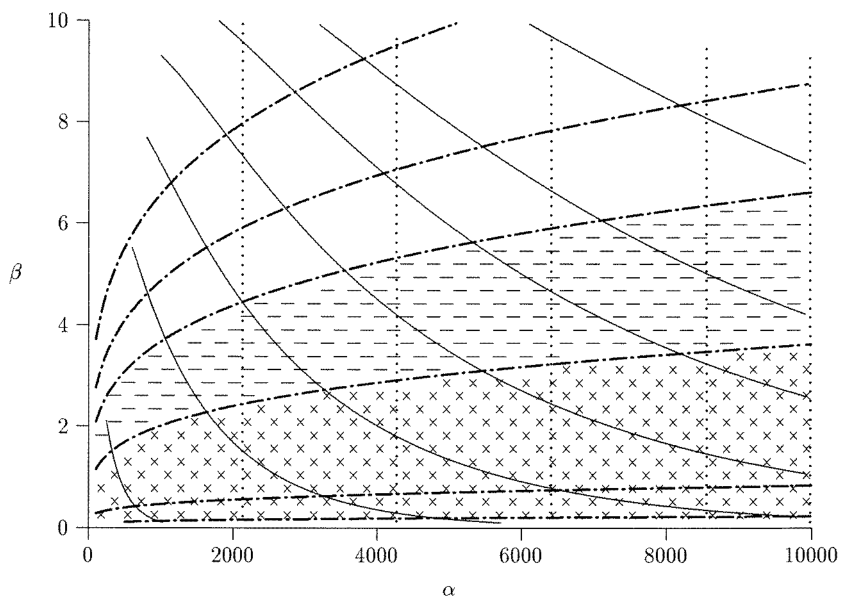

Figure 8. Parameter transformation $(\alpha, \beta) \to (r, T)$, $(p, q, l) = (1, 3, 0)$. Shown are isolines of T $(\cdots\cdots)$, r (——) and $e^{-rT} = e^{-\pi c}$ (— · —). From left: $T = 1500, 3000, 4500, 6000, 7000$. From left: $r = 5 \times 10^{-3}, 10^{-3}, 5 \times 10^{-4}, 3 \times 10^{-4}, 2 \times 10^{-4}, 1.5 \times 10^{-4}$ and 10^{-4}. From top: $e^{-rT} = 0.65, 0.56, 0.47, 0.32, 0.1, 0.003$. The borderline for acceptable quantitative accuracy of the 'asymptotic' Poincaré map is at about $e^{-rT} \approx 0.3$ ($\times$ hatches), the empirical Poincaré map is good up to about $e^{-rT} \approx 0.5$ ($\times$ and $-$ hatches).

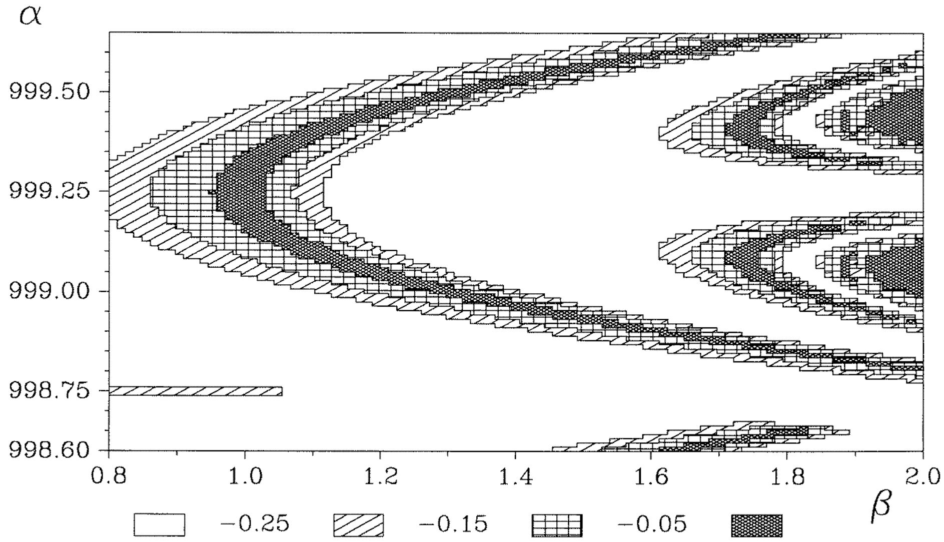

Figure 9. Lyapunov diagram of the one-dimensional map. Hatches denote values of Lyapunov exponents in different intervals as in the legend. The dark shaded areas include values $\gtrsim 0$ of the exponent and indicate bifurcation lines and, at the far right, chaotic regions. The leftmost dark arc covers the first, left–right symmetry breaking bifurcation line; the smaller ones belong to a Feigenbaum-type bifurcation cascade. α axis in 2π units.

where our theory is applicable. The 'tongues' are very nearly periodic in (α, β) parameters. The two-dimensional map predicts their location in the α direction with an absolute error of order 10^{-2} as compared with the diagram directly determined from the differential equation. For values $\beta > 1$, i.e. at the right-hand side of the maps, several attractors with different Lyapunov exponents can coexist, as is easily derived from the map (7). We have made no effort to hit corresponding attractors in each of the two diagrams; this explains the minor differences seen between them. The β coordinate measures—as anticipated—the strength of the nonlinearity effects but not the resonance state. To reach larger values of β at fixed values of α one would have to increase e^{-rT} (figure 8) and thus decrease the adequacy of the map. It is possible, however, choosing α sufficiently large, to cover arbitrary large β values and thus reach highly chaotic states and regimes with multiple attractors. For $\alpha \to \infty$ one could thus construct the complete 'generic' asymptotic tongue.

We have investigated corresponding diagrams for other sets of exponents (p, q, l) permitted by the restriction of equation (13). They all yield similar results. The size of the parameter α necessary to achieve very good applicability of the map varies slightly with the value of the exponents: it increases with increasing q and l.

Next we shall explore possible extensions of our theory into regions of the parameter space where the 'asymptotic' requirements $r \ll 1 \ll T$ and $c = r/\Omega < 1$ are only marginally fulfilled. With practical applications instead of a principal understanding in mind, this could be the more relevant regime. Lyapunov diagrams in the near asymptotic regime (e.g. around $\alpha = 20$, $\beta = 1$, $(p, q, l) = (1, 3, 0)$, which corresponds to $\mathrm{e}^{-rT} \approx [0.2 \ldots 0.5]$, $r \approx [0.01 \ldots 0.02]$, $T \approx 100$) show that the *qualitative* correspondence (as far as Lyapunov diagrams are concerned) between differential equation and Poincaré map is still rather convincing, but not so the *quantitative* correspondence. This is for one or several of the following reasons.

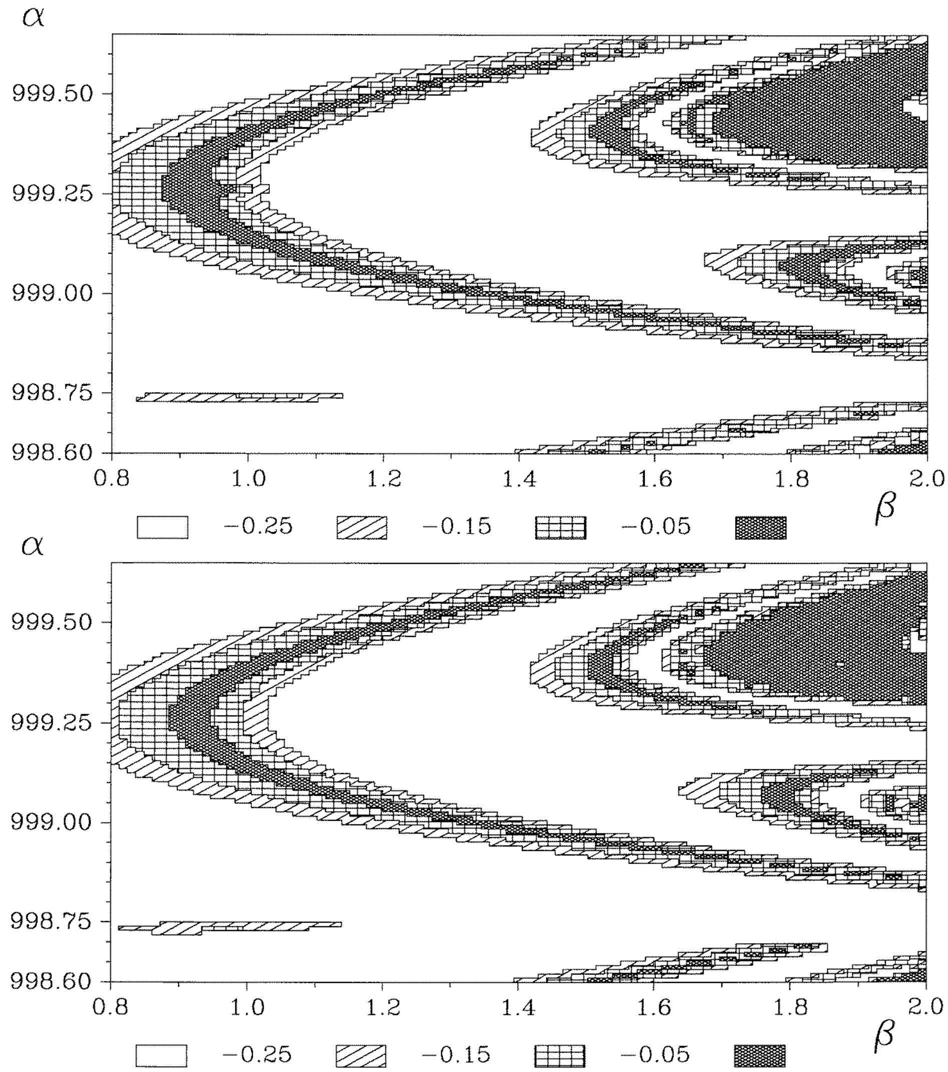

Figure 10. Lyapunov diagram of Duffing's equation (top) and the two-dimensional map (bottom). α-axis in 2π units. Corresponding to the values of (α, β) in this plot, the original parameters vary in the intervals: $e^{-rT} = 0.10 \ldots 0.22$; $r = 0.000\,33 \ldots 0.000\,50$; $T = 4412 \ldots 4418$.

(i) If the expansion parameter e^{-rT} is not small enough, higher orders markedly contribute to the map. This could be remedied by deriving and using higher order terms of the map—a procedure hardly practicable. In any case, if $e^{-rT} \approx 1$ our theory is no longer relevant.

(ii) If T is so small that the overlapping regions II and IV cease to exist, our argument for the existence of 'universal' constants for the map breaks down. Nevertheless the map in its analytic form might still be applicable if corresponding coefficients (possibly slightly parameter dependent) could be determined empirically.

(iii) The latter could also be true if the approximation $x_0 \approx x_m$ breaks down, i.e. region III ceases to be relevant. In this case, the functions $F_\nu(r, \Omega)$ of equation (16) would have to be merged with the 'empirical' coefficients, provided those make sense at all.

In the following we describe a method for using empirical coefficients and reference cycles to replace their 'universal' cousins. This extends the applicability of the Poincaré map to parameter regions where the general mechanism at the basis of our theory still applies, but our derivations for the asymptotic parameter regime become invalid. This method still uses 'fictitious' and 'real' variables similar to the asymptotic case. 'Fictitious' coordinates (i_m, φ_m) at times $t = mT$ are mapped to (i_{m+1}, φ_{m+1}) at times $t = (m+1)T$; 'real' coordinates $(x, \dot{x})$ are used to numerically integrate the system from $t = -T/2$ to $t = T/2$.

Values (I'_a, φ'_a)† are determined by integrating the differential equation with initial conditions $(x(0), \dot{x}(0)) = (-x'_0(T), -\dot{x}'_0(T))$ along the interval $(0, T/2)$. The values of $(y(T/2), \dot{y}(T/2))$ are transformed into action-angle variables at this instant and the latter are extrapolated back into fictitious values (I'_a, φ'_a) at $t = 0$ by use of equation (22).

The other empirical coefficients are then determined according to the following scheme:

$$
\begin{array}{llcccccc}
\text{Real} & (I_n, \varphi_n) & \longrightarrow & (x, \dot{x}) & \rightsquigarrow & (x, \dot{x}) & \longrightarrow & (I_{n+1}, \varphi_{n+1}) \\
\text{Coordinates} & t = -\dfrac{T}{2} & & t = -\dfrac{T}{2} & & t = \dfrac{T}{2} & & t = \dfrac{T}{2} \\
 & \uparrow & & & & & & \downarrow \\
\text{Fictitious} & (i_n, \varphi_n) & & & \text{—Poincaré map} \longrightarrow & & & (i_{n+1}, \varphi_{n+1}) \\
\text{Coordinates} & t = 0 & & & & & & t = T.
\end{array}
$$

Here '$\longrightarrow$' denotes a coordinate transformation, '$\rightsquigarrow$' the integration of a differential equation and $\uparrow\downarrow$ analytical extrapolation as in equation (22). This scheme, applied to a sufficiently large set of conveniently chosen trajectories, proceeds in analogy to the determination of the universal constants in section 3, this time, however, *separately for every single set of parameters* (r, Ω)! In contrast to section 3, there is no patching procedure left. The finitely many 'test' trajectories are numerically integrated from $t = -T/2$ to $t = +T/2$ in the variables $(x, \dot{x})$ and converted via $y = x - x_0$ to action-angle variables precisely at $t = T/2$. At this point, and only there, they are real action-angle variables. These are then extrapolated back and forth into the entire interval $[0, T]$ as in equation (22) to obtain fictitious action-angle variables. Obviously in this case the most suggestive and direct definition of the Poincaré map would be in variables $(I(T/2), \varphi(T/2))$. Its analytic form would be similar to the form (10) but a direct comparison with our asymptotic results would be hindered. Therefore we still define the 'empirical' Poincaré map in fictitious variables $(I(T), \varphi(T))$. The variable i is now defined through

$$I_n(T) = \Omega^{2\gamma+\eta} \mathrm{e}^{-rT} I'_a (1 + \mathrm{e}^{-rT} i_n). \tag{25}$$

If one chooses the initial conditions of the test trajectories on a single circle with fixed i, as we have done here, one can calculate the empirical map coefficients using a Fourier transform which only allows for the five frequencies $\mathrm{e}^{\mathrm{i}n\varphi}$, $n = -2, -1, 0, 1, 2$, which are the ones also contained in the asymptotic map. This will no longer correspond to a strictly systematic expansion in powers of e^{-rT}, since the coefficients will include contributions from higher than second order. As we no longer require e^{-rT} to be *very* small, however, this is a desired effect which increases the accuracy of the map.

For optimal accuracy, the action-angle transformation at $t = T/2$ must take the time dependence of the equation of motion into account, the sources of which are coefficients e^{-2rt} and $x_0(t)$ in the potential of the Hamiltonian version, as described in section 1, of

† We use a dash $'$ to denote parameter-dependent coefficients for the Poincaré map in place of the formerly defined universal constants.

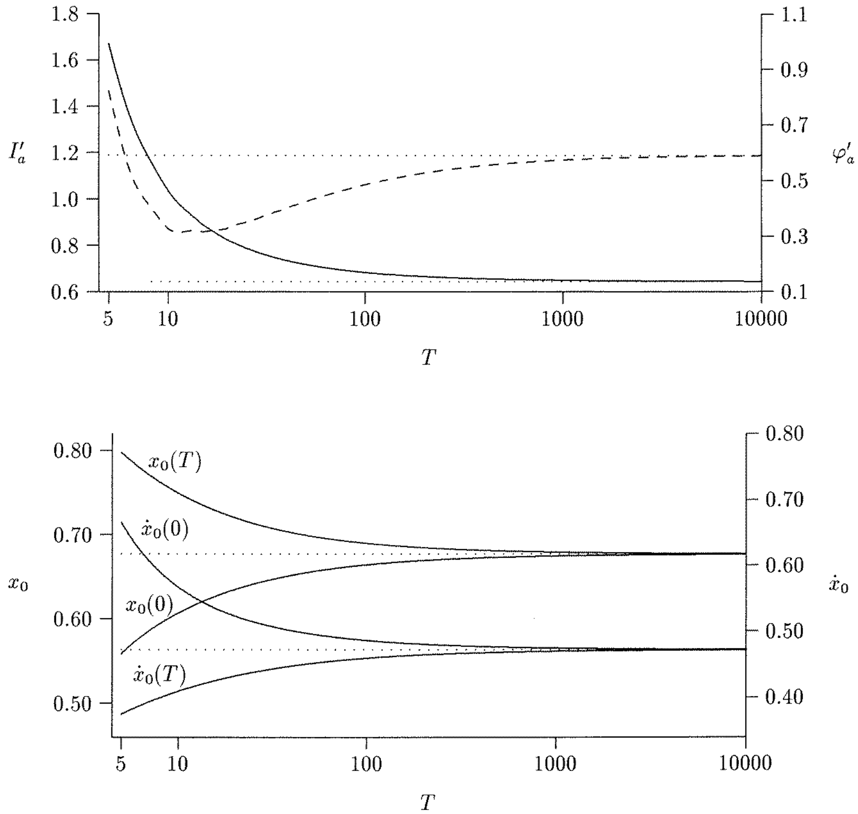

Figure 11. Top: I'_a (——) and φ'_a (– – –) dependent on T, asymptotic values I_a, φ_a $(\cdots\cdots)$. Bottom: Start and end points of the parameter-dependent reference solution $x_0(t)$ in ξ-scaling (——), asymptotic $(\xi_0, \dot{\xi}_0)$ curves $(\cdots\cdots)$. The value of e^{-rT} is held fixed here at 0.2 and thus defines a definite value of r for each T.

the system under consideration. At the instant $t = T/2$, $\dot{x}_0(t)$ is still expected to be negligibly small, but the friction coefficient r may no longer be considered *very* small. The transformation is described in appendix B.

Figure 11 shows how the quantities I'_a, φ'_a, $x'_0(0)$ and $\dot{x}'_0(0)$ determined by the described procedure approach their asymptotic counterparts with increasing T; the other coefficients behave similarly.

The Lyapunov diagrams for the differential equation and Poincaré map to second order with *empirical* coefficients (figure 12) show excellent quantitative agreement also in the accessible non-asymptotic region. The parameter space coordinates used are still the (α, β)-coordinates according to (7). Naturally, the bifurcation tongues are now deformed in comparison to the asymptotic ones and no longer exhibit strict periodicity in the α-direction.

The empirical coefficients were calculated *for every single parameter point* to demonstrate the best possible application. This rather expensive procedure can be relaxed, though, for most applications, since the coefficients vary only slightly in small sectors of parameter space as figure 11 shows.

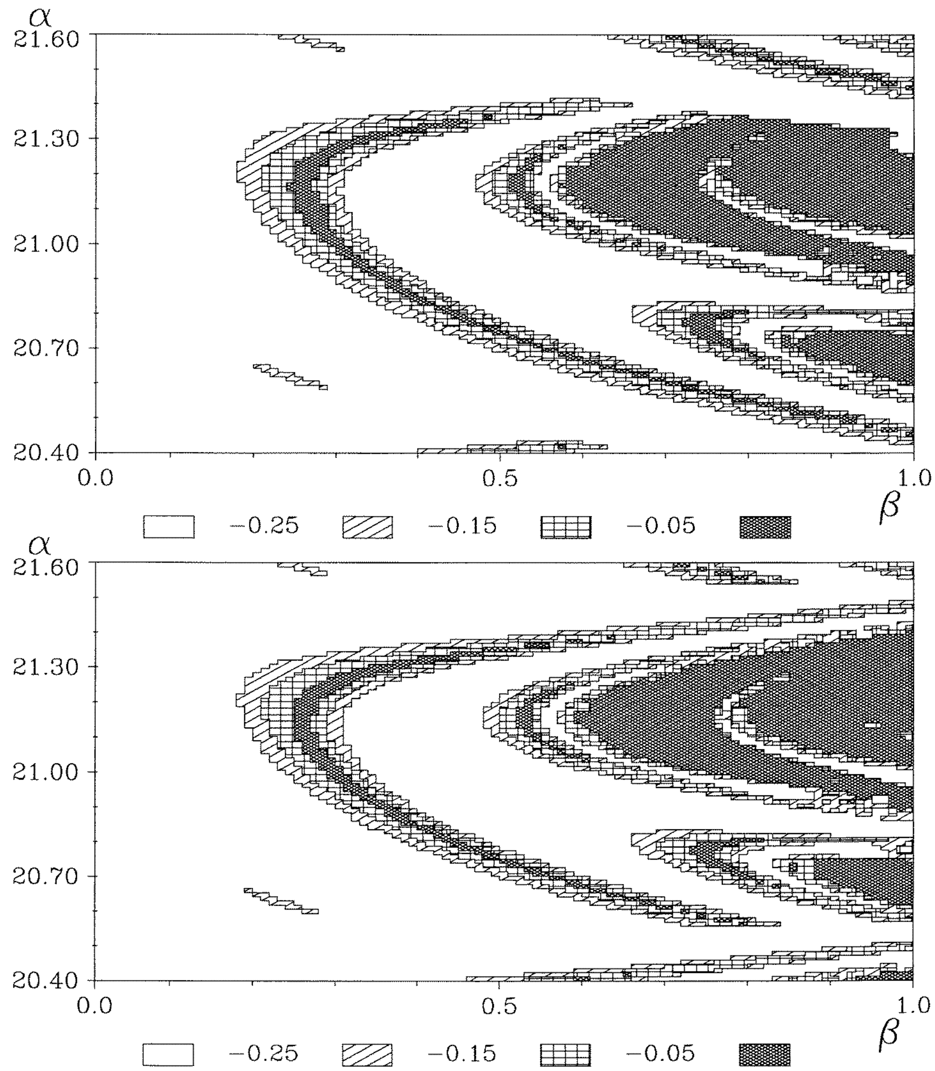

Figure 12. Lyapunov diagram of Duffing's equation (top) with parameters $(p, q, l) = (1, 5, 2)$ and the two-dimensional map (bottom) with (α, β)-dependent map coefficients, α-axis in 2π units. The shape and position of the bifurcation tongues match excellently. The differences between the two figures are caused by the existence of multiple attractors as explained in the text.

5. Conclusions

We presented the methods and technical procedures needed to numerically obtain a quantitative description of the behaviour of Duffing-type oscillators in the limit of large forcing amplitudes through Poincaré maps explicitly available through analytical expressions as derived in paper I. We showed how to separate the motion of these oscillators into the slow motion of special reference trajectories $x_0(t)$ and the damped oscillating motion of the difference amplitude $y(t) = x(t) - x_0(t)$. We constructed the reference trajectories explicitly and plotted examples (figures 4 and 6) for different models and parameter values of Duffing oscillators. We explained how the potential's nonlinearity repeatedly causes the restart of oscillations in the difference system y. We then described the techniques applied to numerically determine the coefficients in the explicit analytic form of the map in action-angle variables. In the asymptotic regime of large forcing and not too small friction these map coefficients do not depend on the parameters of the original system, and thus also allow for explicit description of the parameter dependence of the map.

In the near asymptotic regime, the map coefficients become parameter dependent and are accessible only by numerical calculation for each parameter set separately; but the map is still given explicitly as function of its dynamic (action-angle) variables. We constructed plots of the Lyapunov exponents in the parameter plane for the differential equation and the Poincaré map (figures 9 and 10) which show the excellent quantitative agreement between both in the asymptotic as well as the near asymptotic case. We introduced special coordinates (α, β) in parameter space as physically relevant and convenient. These coordinates lead to phase diagrams which clearly exhibit the resonance tongues as periodically repeated structures in parameter space (in the asymptotic case).

In the near asymptotic regime, we expect the greater *practical* applicability of our theory. The Lyapunov diagrams no longer exhibit strict periodicity, but are still very well amenable to investigation by means of a Poincaré map which allows prediction of system's behaviour depending on parameters. Iterating the Poincaré map instead of integrating the differential equation is particularly relevant if computation time is critical, e.g. with real time applications.

Appendix A. Numerical values of universal constants

Table 1. Universal constants for typical parameter values (p, q, l). The constants A_1 and A_2 are derived from the factors c_ν of equation (6).

	$q = 3$, $p = 1$, $l = 0$	$q = 4$, $p = 1$, $l = 0$	$q = 2.1$, $p = 1$, $l = 0$	$q = 5$, $p = 1$, $l = 2$	$q = 4$, $p = 1.5$, $l = 0$
δ	0.333 333	0.250 000	0.476 190	0.333 333	0.375 000
λ	2.666 666	2.750 000	2.523 809	3.333 333	3.125 000
γ	0.250 000	0.181 818	0.377 358	0.200 000	0.240 000
η	0.250 000	0.272 727	0.207 547	0.400 000	0.360 000
ξ_1	0.677 030	0.740 548	0.568 342	0.690 634	0.629 283
ξ_2	0.472 173	0.389 803	0.603 279	0.412 847	0.485 961
I_a	0.643 386	0.695 257	0.520 835	0.366 509	0.577 521
φ_a	0.590 845	1.170 859	2.252 078	3.020 047	1.874 718
B_1	1.373 153	1.289 717	1.550 786	1.455 937	1.891 013
B_2	0.630 713	0.702 156	0.576 042	1.685 496	1.332 053
B_3	−0.179 346	−0.488 821	0.218 103	−0.971 862	−0.808 882
C_1	1.547 038	2.314 061	3.402 285	3.282 775	3.780 085
C_2	0.804 548	1.639 907	1.492 144	4.576 395	3.741 357
C_3	1.275 581	1.170 801	1.420 545	0.106 784	0.268 957
χ_1	−2.208 157	−2.064 884	−2.429 117	−1.142 350	−1.973 212
χ_2	−3.134 970	−3.045 390	2.933 932	−1.630 484	3.034 903
ψ_1	2.848 043	−2.799 271	−2.817 896	−1.574 090	−2.256 788
ψ_2	2.157 146	2.550 070	2.602 434	−1.720 956	2.826 991
A_1	1.426 348	1.614 111	1.237 579	1.235 253	1.486 087
A_2	−0.375 308	−0.782 164	−0.124 132	−1.832 548	−0.649 711

Appendix B. Time-dependent action-angle transformation

In sections 3 and 4 we encountered the task of converting position–momentum variables at large times into action-angle variables for a system with explicit time dependence. Ideally, this time dependence would be so small that the adiabatic theorem applies and the action I remains constant. To achieve adiabaticity in practice, the numerical requirements on the parameters which determine the time dependence in the Hamiltonian and consequently the requirements on the integration intervals would become extreme. Integration times and lack of numerical accuracy would remain unsatisfying for our purposes. To overcome these difficulties we derived time-dependent canonical transformations which led to a constant action I at times long before the regime of sufficiently slow time dependence is reached. As this region is approached, the transformation approaches the stationary one which was discussed in paper I. Although rather technical, these transformations are indispensable for accurate numerical determination of the coefficients in our Poincaré map. For reproducibility of our results we therefore find it necessary to describe these transformations in some depth.

Since we require a transformation which leads to the equation of motion

$$\dot{I} = -\frac{\partial H}{\partial \varphi} = 0 \tag{26}$$

the momentary frequency must become independent of φ:

$$\dot{\varphi} = \frac{\partial H}{\partial I} = \omega(I, t). \tag{27}$$

The equations of motion for the original Hamiltonian variables (z, p, t), expressed as functions of the variables (I, φ, t) are consequently

$$\begin{aligned} &\frac{\partial z}{\partial t} + \frac{\partial z}{\partial \varphi}\omega(I, t) - p = 0 \\ &\frac{\partial p}{\partial t} + \frac{\partial p}{\partial \varphi}\omega(I, t) + \frac{\partial W(z, t)}{\partial z} = 0. \end{aligned} \tag{28}$$

The total restoring force $\partial W/\partial z$ for our systems of interest can be written as an expansion

$$\frac{\partial W}{\partial z} = \omega_0^2(t) z\left(1 + \sum_{n=1}^{\infty} b_n(t)(v(t)z)^n\right) \tag{29}$$

where certain time-dependent factors $v(t)$ are kept separately for later convenience. The equations (28) are now solved by the following ansatz, which obviously is an expansion into anharmonic corrections:

$$\begin{aligned} z &= -\tfrac{1}{2}\sum_{n=1}^{\infty} v^{n-1} R^n \sum_{k=0}^{n} Q_{n,n-2k}(t) \mathrm{e}^{\mathrm{i}(n-2k)\varphi} \\ p &= -\frac{\mathrm{i}}{2}\omega_0(t)\sum_{n=1}^{\infty} v^{n-1} R^n \sum_{k=0}^{n} P_{n,n-2k}(t) \mathrm{e}^{\mathrm{i}(n-2k)\varphi} \end{aligned} \tag{30}$$

$$\omega(I, t) = \omega_0(t) B \qquad B = 1 + \sum_{1}^{\infty} \beta_{2n}(vR)^{2n} \tag{31}$$

with $R = (2I/\omega_0(t))^{1/2}$.

If this ansatz were inserted without more ado into equations (28), one would obtain differential equations in the independent variable t for the coefficients Q, P and β, which then could be solved order by order ascending with n. These equations leave the coefficients underdetermined, as a consequence of the fact that a time-dependent canonical transformation to action-angle variables leaves the freedom to redefine the angle via $\varphi \to \varphi + \Psi(R, t)$. We use this freedom to impose the following restrictions.

- The coefficients β_{2n} are those of the time-independent transformation, i.e. the coefficients obtained by dropping the time derivative in (28).
- The coefficients $Q_{2n+1,1}$ are real.
- All coefficients are to approach the corresponding ones of the time-independent transformation in the adiabatic limit.

This strategy was used in two different contexts as follows.

B.1. Patching operation

As described in section 3, we had to patch together numerical solutions to analytical solutions in a region where the reference solution was given by the asymptotic expression from equation (17):

$$\xi_0(t) = t^\delta\left(1 + \sum_1^\infty h_n w^{2n}\right) \tag{32}$$

with known coefficients h_n (see below for definition of w). In comparison to equation (29) we obtain

$$\begin{aligned} \frac{\partial W}{\partial z} &= (z+\xi_0)^q - \xi_0^q - t^p((z+\xi_0)^l - \xi_0^l) \\ &= \omega_0^2(t) z\left(1 + \sum_1^\infty b_\nu \left(\frac{z}{\xi_0}\right)^\nu\right) \end{aligned} \tag{33}$$

where

$$\begin{aligned} \omega_0^2(t) &= q\xi_0^{(q-1)} - t^p l \xi_0^{l-1} \\ &= \tilde{\omega}_0^2 t^{(q-1)\delta}(1 + w^2 S) \end{aligned} \tag{34}$$

$$b_\nu(t) = \frac{1}{\omega_0^2}\left[\binom{q}{\nu+1}\xi_0^{q-1} - t^p \binom{l}{\nu+1}\xi_0^{l-1}\right] \tag{35}$$

and S and b_ν turn out to be asymptotic series in the variable w starting with a term $\sim w^0$. We eliminate prefactors according to

$$w = \frac{\mathrm{i}}{\tilde{\omega}_0} t^{-\kappa} \qquad \tilde{\omega}_0 = (q-l)^{1/2} \qquad \kappa = 1 + \frac{q-1}{2}\delta \tag{36}$$

$$z = t^{-\frac{q-1}{4}\delta}\tilde{z} \qquad p = t^{\frac{q-1}{4}\delta}\tilde{\omega}_0 \tilde{p} \qquad R = t^{-\frac{q-1}{4}\delta}\left(\frac{2I}{\tilde{\omega}_0}\right)^{1/2} \tag{37}$$

$$v = t^{-\mu} \qquad \mu = \frac{q+3}{4}\delta \tag{38}$$

to obtain

$$\begin{aligned} &B\frac{\partial \tilde{z}}{\partial \varphi} + \mathrm{i}w\left(D + \frac{q-1}{4}\delta\right)\tilde{z} - \tilde{p} = 0 \\ &B\frac{\partial \tilde{p}}{\partial \varphi} + \mathrm{i}w\left(D - \frac{q-1}{4}\delta\right)\tilde{p} + \tilde{z}\left(b_0 + \sum_1^\infty b_\nu (v\tilde{z})^\nu\right) = 0 \end{aligned} \tag{39}$$

$$D = \mu v\frac{\partial}{\partial v} + \kappa w \frac{\partial}{\partial w} = -t\frac{\partial}{\partial t}. \tag{40}$$

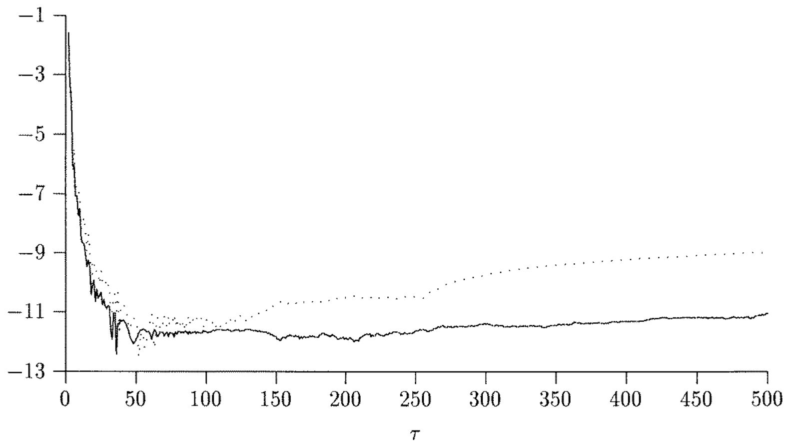

Figure B1. Time dependence of the values I_a and φ_a obtained by integration of the equation $\ddot{\xi} + \xi^3 + \tau = 0$ and time-dependent action-angle transformation as described in appendix B.1. The graph shows $\log|I_a - I_\tau|$ and $\log|\varphi_a - \varphi_\tau|$ where I_τ and φ_τ are the values determined by using the action angle transformation at the instant τ. The figure shows that the values (I_τ, φ_τ) stay constant up to 11 digits for times τ larger than 30. The increase of the deviation for larger values of τ is caused by rounding errors during integration of the differential equation (accuracy 10^{-14}). The values (I_a, φ_a) were determined at $\tau = 200$ with an accuracy of 10^{-18}. The deviations do not reach zero because of this limited numerical accuracy.

The operator D acting on terms $R^n v^{n-1} w^j$ just adds prefactors $\mu(n-1)+\kappa j$. The coefficients P and Q can now be expanded as series

$$P_{n,k} = \sum_{j=0}^{\infty} p_{n,k,j} w^j \qquad Q_{n,k} = \sum_{j=0}^{\infty} q_{n,k,j} w^j \tag{41}$$

and the coefficients p and q recursively determined.

Note that the imaginary i cancels from equations (39) (thus the coefficients p and q can be taken to be real) and that D is preceded by a prefactor w in (39) with the consequence that the time dependence of the transformation vanishes in the asymptotic limit.

Technically we determined the coefficients p, q and β with the help of computer algebra to order 10 in R and w; similarly the inversion of the transformation as

$$R\mathrm{e}^{\mathrm{i}\varphi} = \sum C_{\mu,\nu,j} \left(\frac{\mathrm{i}p}{\omega_0}\right)^{\nu} z^{\mu} w^j. \tag{42}$$

The quantities I_a and φ_a as determined by help of this transformation are shown in figure B1 as functions of the interval t used for numerical integration.

B.2. Empirical Poincaré map

In this case we use canonical transformations into action-angle variables at the instant $t = T/2$. In the Hamiltonized version for the y-system the position variable is decorated everywhere by a factor e^{-rt}, the time dependence of which is not necessarily negligible. On the other hand, the time dependence of the reference solution x_0 is negligible in the vicinity of $t = T/2$. Thus we have

$$\frac{\partial W(z,t)}{\partial z} = \omega_0^2 z \left(1 + \sum_{n=1}^{\infty} b_n \left(\frac{\mathrm{e}^{-rt}}{x_0} z\right)^n\right) \tag{43}$$

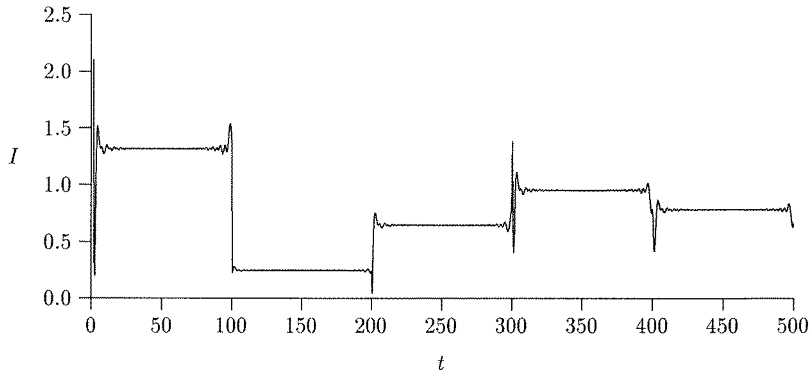

Figure B2. $I(t)$ determined by the time-dependent action-angle transformation as in appendix B.2 for Duffing's equation $(p, q, l) = (1, 3, 0)$ with parameters $r = 0.01$, $T = 100$ resp. $\alpha = 140$, $\beta = 1.5$. This transformation keeps $I(t)$ constant only in the vicinity of the instants $(n+\frac{1}{2})T$. The oscillations near the 'kicks' at $t = nT$ are a result of the time dependence of $x_0(t)$ which was not accounted for.

where the quantities (with $x_0(T/2)$)

$$\omega_0^2 = x_0^{q-1}(q - lx_0^{l-q}) - r^2 \tag{44}$$

$$b_\nu = \frac{\binom{q}{\nu} - \binom{l}{\nu}x_0^{l-q}}{q - lx_0^{l-q} - x_0^{1-q}r^2} \tag{45}$$

are now treated as time independent. This time we substitute

$$v = \frac{\mathrm{e}^{-rt}}{x_0} \qquad t\frac{\partial}{\partial t} \to -rv\frac{\partial}{\partial v} \tag{46}$$

and determine the coefficients Q and P as power series in the (now time independent) variable

$$w = \frac{\mathrm{i}r}{\omega_0} \tag{47}$$

with real coefficients p and q, in analogy to the previous case (including the inverted transform). Figure B2 shows the behaviour of the action I for some typical solution as determined by this method from the numerical solution in x-coordinates. It shows that the action is constant in quite a reasonable vicinity of the instants $(n + 1/2)T$.

References

[1] Eilenberger G and Schmidt K 1992 Poincaré maps of Duffing-type oscillators and their reduction to circle maps: I. Analytic results *J. Phys. A: Math. Gen.* **25** 6335–56

[2] Berger M S and Chen Y Y 1991 Forced quasiperiodic and almost periodic oscillations on nonlinear Duffing Equations *Nonlinear Anal. Theory Methods Appl.* **19** 249–57

Norris J W 1992 Boundedness in periodically forced second order conservative systems *J. London Math. Soc.* **45** 97–112

Huaizhong W and Yong L 1992 Existence and uniqueness of periodic solutions for Duffing equations across many points of resonance *J. Diff. Eqns* **108** 152–69

Berger M S and Zhang L 1994 A new method for large quasiperiodic nonlinear oscillations with fixed frequencies for the nondissipative forced Duffing equation *Panamerican Math. J.* **4** 1–21

Vujanovic B D 1995 Conservation-laws and reduction to quadratures of the generalized time-dependent Duffing equation *Int. J. Nonlinear Mech.* **30** 783–92

Gravador E, Thylwe K E and Hokback A 1995 Stability transitions of certain exact periodic responses in undamped Helmholtz and Duffing oscillators *J. Sound Vibrat.* **182** 209–20

[3] Guckenheimer J and Holmes P 1983 *Nonlinear Oscillations, Dynamical Systems, and Bifurcations of Vector Fields (Applied Mathematical Sciences 42)* (Berlin: Springer) p 82

Gottwald J A, Virgin L N and Dowell E H 1990 Experimental mimicry of Duffing's equation *J. Sound Vibrat.* **158** 447–67

Permann D and Hamilton I 1992 Wavelet analysis of time-series for the Duffing oscillator—The detection of order within chaos *Phys. Rev. Lett.* **69** 2607–10

Lansbury A N, Thompson J M T and Stewart H B 1992 Basin erosion in the twin well Duffing oscillator: two distinct bifurcation scenarios *Int. J. Bifurcation Chaos Appl. Sci. Eng.* **2** 505–32

Belogortsev A B, Poliashenko M and Tretyakov O A 1993 Routes to chaos in bistable systems during multiple crossings of a region of hysteresis *Int. J. Bifurcation Chaos Appl. Sci. Eng.* **3** 405–15

El-Abbasy E M 1994 Oscillatory behaviour of solutions of forced second order differential equations with alternating coefficients *Appl. Math. Comput.* **60** 1–13

Stewart H B, Thompson J M T, Ueda Y and Lansbury A N 1995 Optimal escape from potential wells—patterns of regular and chaotic bifurcation *Physica* **85D** 259–95

Dowell Earl H and Katz A L 1996 A basic explanation of homoclinic intersection in the twin-well Duffing oscillator *Fields Inst. Commun.* **9** 65–92

[4] Gilmore R and McCallum J W L 1994 Structure in the bifurcation diagram of the Duffing oscillator *Phys. Rev.* E **51** 935–56

[5] Zhu W Q, Lu M Q and Wu Q T 1991 Stochastic jump and bifurcation of a Duffing oscillator under narrow band excitation *J. Sound Vibrat.* **165** 285–304

Ravindra B and Mallik A K 1993 Stability analysis of a non-linearly damped Duffing oscillator (Academic) pp 708–16

Koliopulos P K and Langley R S 1993 Improved stability analysis of the response of a Duffing oscillator under filtered white noise *Int. J. Nonlinear Mech.* **28** 145–55

Surajit S and Phillips J C 1995 Relaxation in a Duffing potential *Physica* **216A** 271–87

[6] Berger M S and Chen Y Y 1992 Forced quasi-periodic and almost periodic oscillations of nonlinear Duffing equation *Nonlinear Anal. Theory Meth. Appl.* **19** 249–57

Yang J, Qu Z and Hu G 1996 Duffing equation with two periodic forcings: the phase effect *Phys. Rev.* E **53**

[7] McCartin B 1992 An alternative analysis of Duffing's equation *SIAM Rev.* **34** 482–91

Kao Y H, Wang C S and Yang T H 1992 Influences of harmonic coupling on bifurcations in Duffing oscillator with bounded potential wells *J. Sound Vibrat.* **159** 13–21

Belogortsev A B 1992 Bifurcations of tori and chaos in the quasiperiodically forced Duffing oscillator *Nonlinearity* **5** 889–97

Belogortsev A B 1992 Quasiperiodic resonance and bifurcations of tori in the weakly nonlinear Duffing oscillator *Physica* **59D** 417–29

Vaneck T 1994 The hyper volume method: Finding boundaries between regular and chaotic phenomena in the forced Duffing oscillator *J. Sound Vibrat.* **175** 570–6

Friswell M I and Penny J E T 1994 The accuracy of jump frequencies in series solutions of the response of a Duffing oscillator *J. Sound Vibrat.* **169** 261–9

[8] Szemplinska-Stupnicka W 1994 A discussion of a analytical method of controlling chaos in Duffing's oscillator *J. Sound Vibrat.* **178** 276–84

Kivshar Y S, Rödelsperger F and Brenner H 1994 Supression of chaos by nonresonant parametric pertubations *Phys. Rev.* E **49** 319–24

Nijmeijer H and Berghuis H 1995 On Lyapunov control of the Duffing equation *IEEE Trans. Circ. Syst. I Fund. Theory Appl.* **42** 473–7

Alvarez-Ramirez J, Femat R and Gonzalez J 1996 A time delay coordinates strategy to control a class of chaotic oscillators *Phys. Lett.* A **211** 41–5

Sass B and Toroczkai Z 1996 Continuous extension of the geometric control method *J. Phys. A: Math. Gen.* **29** 3545–57

[9] Kozlowski J, Parlitz U and Lauterborn W 1995 Bifurcation analysis of 2 coupled periodically driven Duffing oscillators *Phys. Rev.* E **51** 1861–7

Ashwin P 1995 Weak coupling of strongly nonlinear, weakly dissipative identical oscillators *Dyn. Stab. Syst.* **10** 203–18

Leung A Y T and Chui S K 1995 Non-linear vibration of coupled Duffing oscillators by an improved incremental harmonic balance method *J. Sound Vibrat.* **181** 619–33

Sen T, Ellison J A and Kauffmann S K 1995 Collective behaviour of an ensemble of forced Duffing oscillators near the 1/1-resonance *Physica* **81D** 44–78

[10] Stefanescu I S 1990 The Duffing equation at large forcing and damping *Preprint* Universität Karlsruhe TKP 90-11

[11] Ueda Y 1980 Steady motions exhibited by Duffing's equation: a picture book of regular and chaotic motion *New Approaches to Non-linear Problems in Dynamics* ed P J Holmes (Philadelphia, PA: SIAM)

Ueda Y 1992 *The Road to Chaos* (Santa Cruz, NM: Aerial)

[12] Parlitz U and Lauterborn W 1985 Superstructure in the bifurcation set of the Duffing equation *Phys. Lett.* **107A** 351–5

Zeni A R and Gallas J A C 1995 Lyapunov exponents for a Duffing oscillator *Physica* **89D** 71–82

Van Dooren R and Janssen H 1996 A continuation algorithm for discovering new chaotic motions in forced Duffing systems *J. Comput. Appl. Math.* **66** 527–41

[13] Feigenbaum M J 1980 Universal behaviour in nonlinear systems *Los Alamos Sci.* **1** 4–27

[14] Schmidt K and Eilenberger G 1998 *A Program Suite for the Analysis of Duffing's equation supplemented by: XDOC, a Program Documentation System* (Internal report, available from the authors and from server http://www.kfa-juelich.de/iff/theory1/duffing/index.html)

[15] Levin D 1973 Development of non-linear transformations for improving convergence of sequences *Int. J. Comput. Math.* B **3**